

Modal Analysis of Alkali Activated Slab Degraded by Ultraviolet Light

DVOŘAK R.^{1,a}, TOPOLÁŘ I.^{1,b}, PAZDERA L.^{1,c}, BÍLEK V.^{2,d},
HRUBÝ P.^{2,e}, PLSKOVÁ I.^{1,f}

¹Institute of Physics, Faculty of Civil Engineering, BUT – Brno University of Technology, Brno University of Technology, Veveří 331/95 602 00 Brno, Czech Republic

²Institute of material science, BUT – Brno University of Technology, Purkyňova 464/118, Královo Pole, 61200 Brno 12

^advorak.r1@fce.vutbr.cz, ^blibor.topolar@vutbr.cz, ^cpazdera.l@fce.vutbr.cz, ^dbilek@fch.vut.cz, ^exchrubyp@fch.vut.cz, ^fplskova.i@fce.vutbr.cz

Keywords: Modal analysis, frequency response function, materials, alkali activated systems, non-destructive testing

Abstract. In the field of vibroacoustic testing methods an experimental modal analysis is vastly used, which allows inspecting natural frequencies and damping ratios of test specimens. In the literature a numerous approach is being used for laboratory testing setups which mostly consist of an elastic suspension of test specimen and usage of different types of accelerometers, shakers, and modal hammers. The presented paper focuses on the comparison of different test setups of used sensors and impact exciting of a test specimen of slab made of alkali-activated slag mortar, which was degraded by ultraviolet light. The paper aims to find optimal setup combination for testing of such material by experimental modal analysis and decide if ultraviolet light alter the vibroacoustic properties of test specimens.

Introduction

Based on statistics across the globe, the main construction material used in civil engineering is concrete [1-4], where main used binder component is cement. The manufacturers are pushed to reduce the amount of released CO₂ per ton of cement. either partial substitution of clinker by secondary raw latent hydraulic additives (such as blast granulated slag, fly ash etc.) or usage of completely different binders.

Alkali-activated systems represent applicable alternative binder to conventional cement. Such material has advantage in the utilization of secondary raw materials and much lower input energy and carbon dioxide emissions compared to the manufacturing of Portland cement. Although it is relatively well-known material [5], its usage in the industry is still limited to prefabricated elements and monolithic structures mostly in Ukraine [6]. Alkali-activated materials are formed by the reaction between suitable alumina-siliate precursors with an alkaline solution. The whole process of alkaline activation starts with the dissolution of the reactive precursor particles in highly alkaline environment and continues with the nucleation and poly-condensation reactions to form main hydration products like C-A-S-H in case of alkali-activated blast furnace slag or N-A-S-H for the alkali-activation of fly ash. The hydration products formed are amorphous or semi-crystalline. Some minor crystalline phases can also be found with dependence of alumino-silicate precursor composition [7]. Spatially crosslinked

structure of C-A-S-H gels is produced by this reaction [8], which leads to more homogenous and partially amorphous structure apart to crystalline structure of cement stone.

Testing of such material consists mainly of physical-mechanical and physical-chemical procedures. One of the yet unknown property of this composite is its resistance to ultra-violet radiation. The presented paper consists of an experiment of preparation of 4 test specimens of alkali-activated mortar of dimension 320×82×19 mm, which were substituted to cycling for 200 and 268 days of UV radiation, change of temperature and humidity in the QUV-Sun [9].

Test specimens were stored in QUV chamber from 7.8.2019 to 19.02.2020 and the specimens were subjected to UV radiation for 6432 hours. The chamber individual cycle consists of 4 hours of UV radiation of intensity 0.89 W/m² at temperature 60 °C and 4 hours of water condensation at temperature 50 °C.

Degradation in QUV chamber is mostly used on polymers, exterior facade elements etc. for fast aging procedures. Similar measurement on alkali-activated specimens is fairly narrow or even non-existing among the scientific papers. As an example can be presented study which used UV chambers for accelerated aging of resin treated concrete surface [10]. The conclusion of cited paper sums, that concrete itself is quite durable in terms of UV degradation, and the only part which suffers are polymer coatings. It is therefore expected that alkali-activated composite will behave similar to standard concrete.

Designed mixture

The mixture composition is based on alkali-activation of granulated blast furnace slag (GBFS). The GBFS was obtained by Kotouč Štramberk Ltd., from city Štramberk in Czech Republic. The GBFS composition determined by XRF is shown in Table 1. It had a specific surface area according to Blaine about 400 m²·kg⁻¹. A fine aggregate of siliceous sand of three different fractions with maximal grain size 2 mm is used according to the EN 196-1. The 50% solution of sodium hydroxide in dosage of 6% Na₂O by the slag weight was used as an alkaline activator. Water to slag ratio (including extra added water and water from activator) was 0.45. To achieve the desired workability, the commercial superplasticizer based on lignosulfonates (ChrysoPlast 461) was used in 1% dose with respect to the slag weight.

Table 1. The BFS chemical composition (XRF)

Chemical composition in wt. %									
CaO	SiO ₂	MgO	Al ₂ O ₃	SO ₃	TiO ₂	K ₂ O	MnO	Na ₂ O	Fe ₂ O ₃
41.1	34.7	10.5	9.1	1.4	1.0	0.9	0.6	0.4	0.3

Firstly a liquid components with slag were mixed for 3 minutes, and afterwards the sand was added to mixture. Whole mixing took 9 minutes. De-molding of test specimens stored in autogenous conditions (sealed with stretch foil) took place 24 hours after the mixing under the autogenous conditions at temperature circa approximately 25 °C.

Used methods

The specimens were tested before and after the degradation by experimental modal analysis. In the evaluation a natural frequencies N_f and damping ratios ζ_i are compared. Testing setup is illustrated in Figure 1. Test slabs of diameters 0.320×0.082×0.019 were placed on two rubber pads in the transverse direction. There were 4 test slabs in total, which were divided into two groups. First group with specimens names A and B was placed in the QUV testing chamber facing by bottom surface to the source of ultraviolet light and second group with specimens names C and D was facing by upper surface to the source of ultraviolet light.

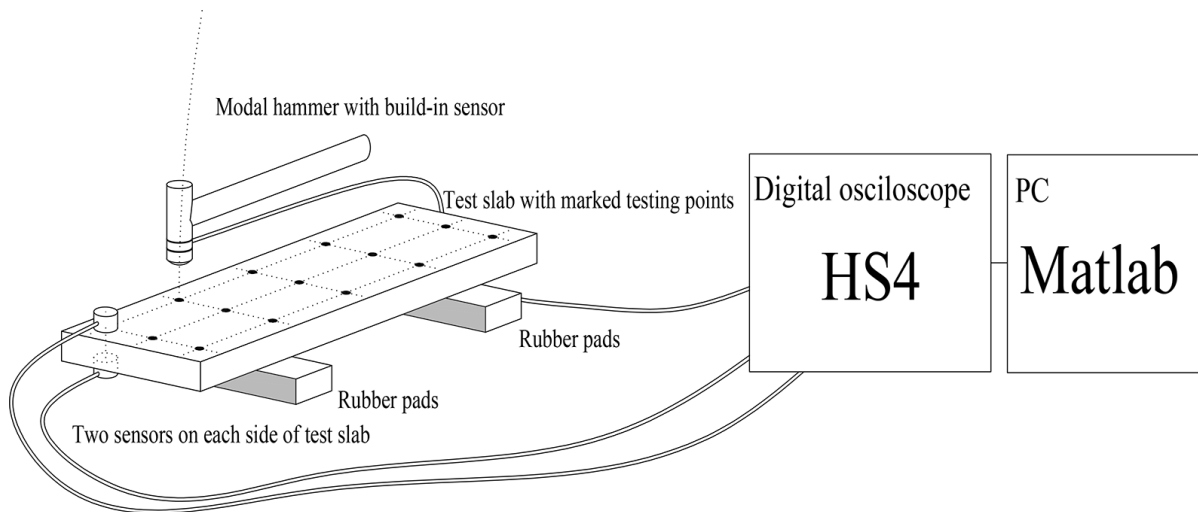


Figure 1: Testing setup

During testing two piezoelectric accelerometers were used, one attached to upper side, and second attached to bottom side of the test slab. For impacting the test specimen, a modal hammer with build-in force sensor was used. Both surfaces of testing slab were divided to 15 testing points, where first point was occupied by receiving sensor on both sides. Each testing point was then impacted three times. After all testing points were tested, the test specimen was turned upside down, and the same measurement was done on the other side. For each testing point an input signal from hammer sensor and response signals from both upper and bottom receiving sensors attached to test specimen were recorded.

For the data acquisition a digital oscilloscope HS4 was used. The sampling frequency of board was set to 195 KHz in 16-bit resolution. Each measured signal consists of $65 \cdot 10^3$ samples and is 0.3 s long with 5% pretrigger. Sensors were attached to the surface of test specimens by beeswax, which is most common approach in vibroacoustic testing in civil engineering materials.

During computing of frequency response function [11], a signal recorded by build-in hammer sensor and signal of receiving sensor attached to surface of test specimens are used for estimation of natural frequencies and damping ratios. In this specific measurement we approach to the whole process as a Single Input-Single Output (SISO) state, despite the possibility of usage of Single Input-Multiple Outputs (SIMO) approach. This is done mainly to compare the resulting estimated natural frequencies in all combination. For processing of measured data, a Matlab software was used, precisely Signal Processing Toolbox and its frequency response function [12] and for extraction of natural frequencies and damping ratios a stabilization diagram function was used [13].

By the used setup we receive in total 8 combination of used signals from hammer and sensor for each degradation state of test specimen. The resulting interpretation of results then focus on the analysis of natural frequencies before and after the degradation of test specimens by ultraviolet light, and comparison of used testing setup and its influence on success rate of natural frequencies retrieving.

Results of testing

The procedure of retrieving of natural frequencies and damping ratios of each testing specimen consist of several steps, which will be described on the example of one test specimens. The final table of retrieved natural frequencies sums up all conducted measurements along with the table comparing all used testing setups.

Example of exciting signal from model hammer and signal measured by both sensors is illustrated at Figure 2. This example shows situation where impacts were aimed at the upper surface of the test specimen. This side is uneven, which is mainly caused by the way the test specimens are manufactured in the mould. By this standard procedure specimens has even surface on sides and bottom surface, but upper surface might suffer on the presence of pores, cracks and other defects, which can influence the testing. As expected, the signal from upper sensor has higher amplitude, then sensor from lower surface. [14]

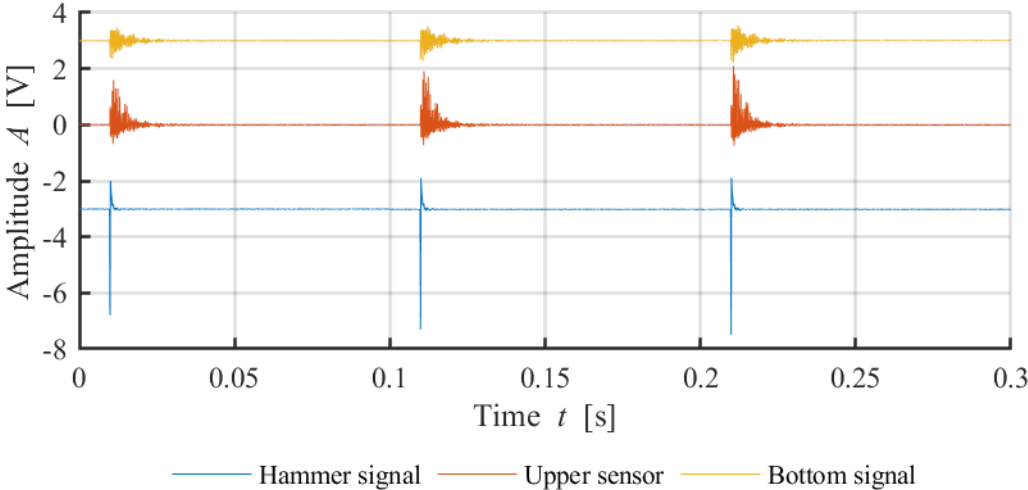


Figure 2: Example of hammer signal and signal response from upper and bottom sensor

From the acquired signals a frequency response function is obtained using Welch’s method using least-squares complex exponential (LSCE) algorithm [15]. An example of magnitude and phase of measurement from first row and first column of testing grid is shown on Figure 3. Subsequent localization of present normal frequency modes and their damping ratios are retrieved using subspace method.

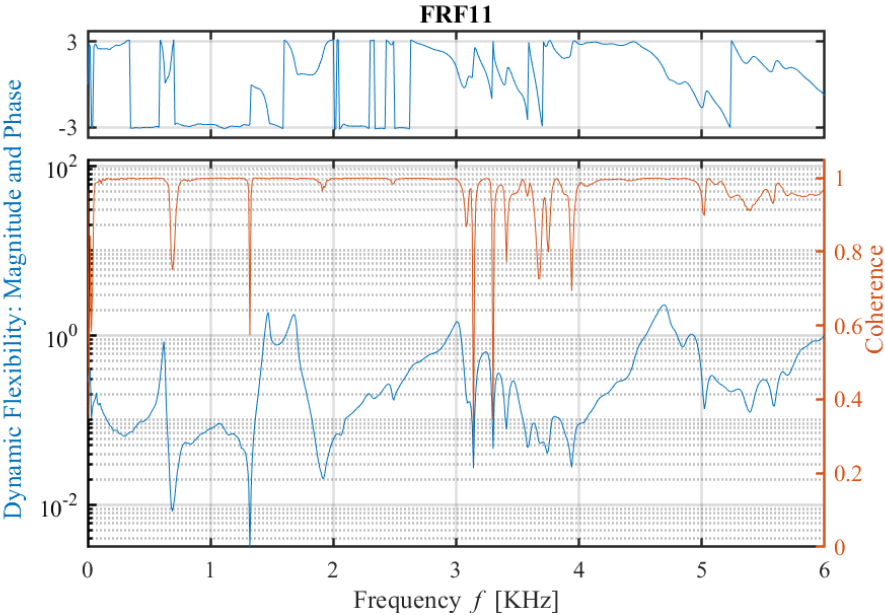


Figure 3: Frequency response function of acquired signals (first column, first row of testing grid on upper side)

The subspace aliased method is fairly used for estimation of modal shapes [16-18]. Example of stability diagram with localized natural frequency modes is shown on Figure 4. In modal analysis, a stabilization diagram is an important tool that is often used to assist the user in separating the physical system poles from mathematical ones [19]. Each given pole is classified as stable in frequency if its natural frequency changes by less than 0.01% as the model order increases. Classify a given pole as stable in damping if the damping ratio estimate changes by less than 0.2% as the model order increases [20]. In the present study the number of localized mode order was upon the initial testing set to 30.

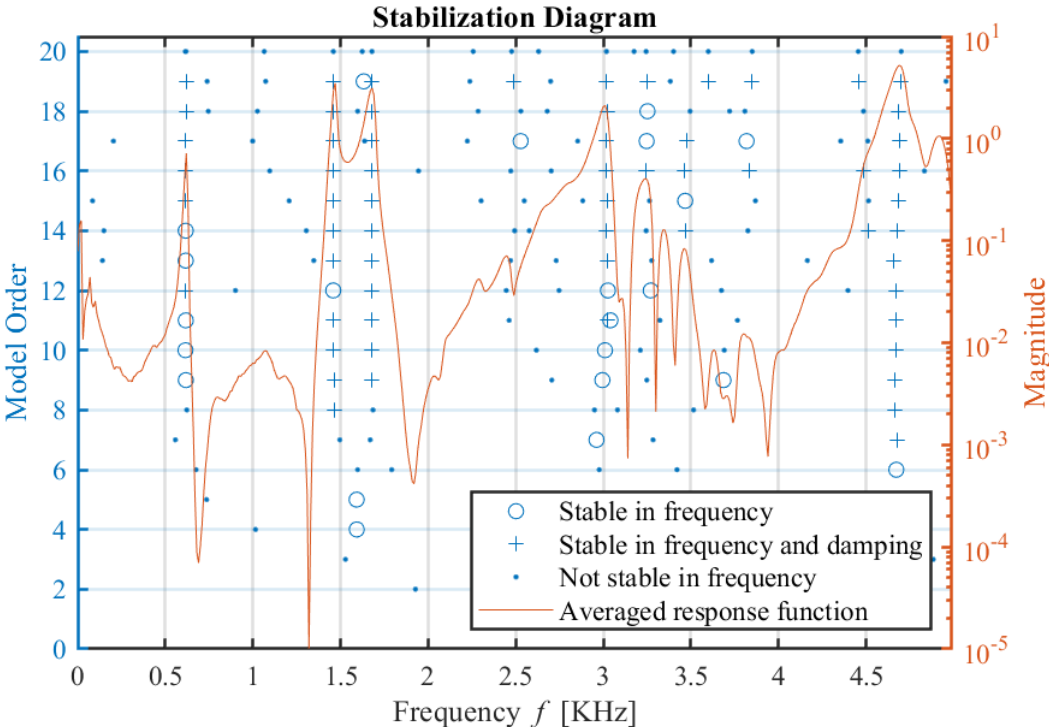


Figure 4: Estimation of stable frequencies of single testing position

The stabilization diagram clearly shows automatically localized natural stable frequencies. Histogram of damping ratios of all conducted tests shown at Figure 5 illustrates damping ratios of all localized frequency modes from all testing points of upper and bottom side of test specimens.

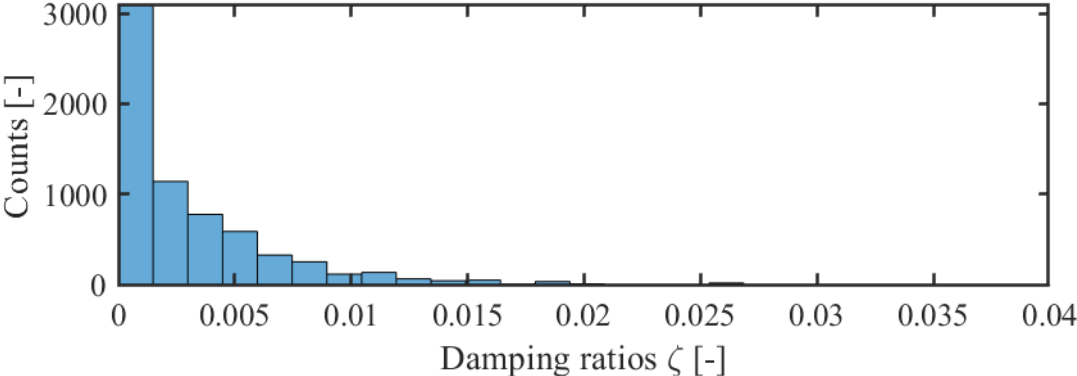


Figure 5: Histogram of damping ratios

The measured natural frequency modes exhibit relatively low damping ratio with exponential distribution across all conducted measurements. Most of the localized natural frequencies are very stable, and for next interpretation only natural frequencies with damping ratios below 0.02 are compared. By this step, we compare only stable modal shapes.

Frequencies retrieved from stabilization diagram and filtered by damping ratios threshold are then stacked up from all different setups for each testing specimen. Given by subspace method processing, each mode shape is represented by different amount of the close values of specific frequency [21-22]. Different measuring setups can result in different amount of detected stable frequency values; thus, each setup can be compared by number of individual frequency values that are parts of each stable natural frequency mode. The Figure 6 compares all frequencies from testing of specimen C, where dots represent each setup combination consisting of side of test specimen, which was degraded, surface which was impacted by modal hammer and receiving sensor, whom signal was used for frequency estimation by subspace method.

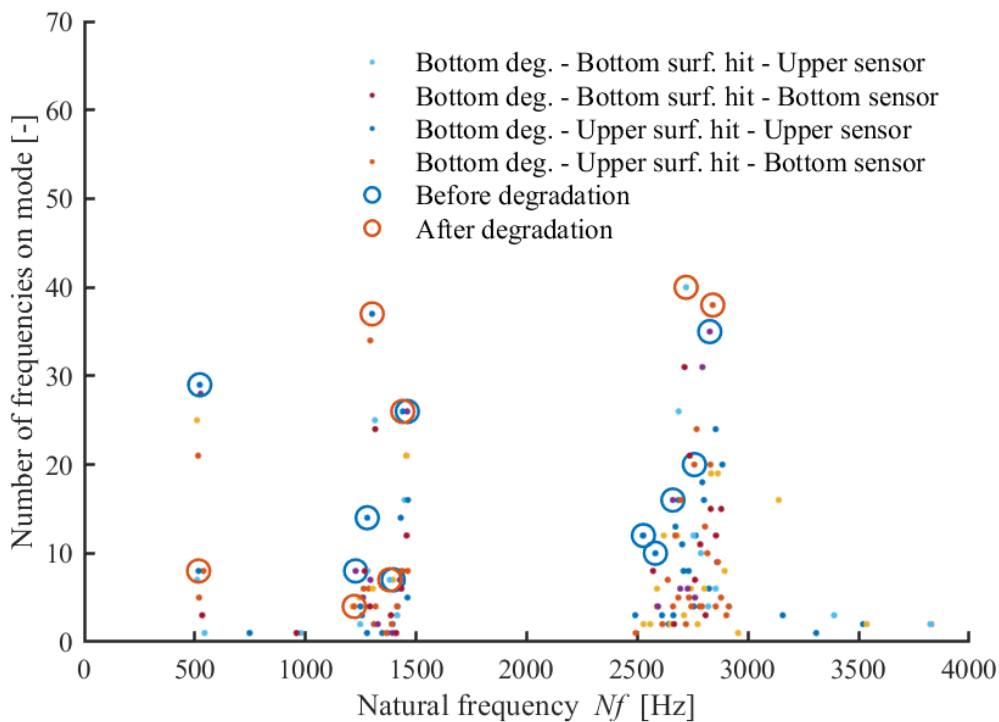


Figure 6: Example of natural frequency histograms of all testing combinations for test specimen C; marked frequencies are dominant in reference and degraded state of sample

The rings then illustrate which frequencies consist of highest amount of values of each state before and after the degradation by UV light. This process was used on all measurements which results in first 10 frequency modes of each specimen before and after the degradation.

For modal analysis computed in Ansys was used poisson ratio equal to 0.2, density of material to $2320 \text{ kg}\cdot\text{m}^{-3}$ and dynamic modulus of elasticity to 1100 GPa. These material characteristics were measured in past publication [23]. Subsequently first ten frequency modes are compared with first ten modes obtained from experimental modal testing, in type of setup hit-sensors which had highest frequency counts based on Figure 6.

Table 2: Exported natural frequencies before and after the degradation with comparison of natural frequencies obtained from ANSYS model

n	Mode frequencies Nf [Hz] of test specimens								ANSYS
	A		B		C		D		
	before	after	before	after	before	after	before	after	
1	636	653	645	672	525	593	539	607	697
2	1482	1518	1367	1485	1262	1304	1280	1472	1581
3	1665	1764	1493	1540	1314	1377	1383	1582	1884
4	2933	1853	1678	1790	1446	1453	1436	1664	2479
5	3013	2282	1776	1919	2682	2657	1961	2980	3226
6	3069	3094	2142	3178	2735	2711	2383	3034	3589
7	3262	3163	2422	3445	2808	2816	2495	3139	4992
8	3331	3354	3069	4889	2893	2922	2646	3200	5536
9	4548	3437	3193	4940	4059	4141	2706	4586	5620
10	4671	4817	3264	4995	4165	4221	2804	4666	5723

At the table 2, for each test specimen is present state before and after the degradation by UV light. At all frequency modes we can observe a slight increase in first three frequency modes, in range 2-12 %. Natural frequencies obtained from Ansys model are higher than measured natural frequency modes in real specimens, but if we compare first frequency mode with average first frequency modes of all specimens, the difference is 0.33%, which is almost negligible difference. Higher frequency modes are much different from Ansys model with average difference in range 6-18%. The further optimization of Ansys model could lead to estimation of body stiffness of tested specimens and other material mechanical properties.

Table 3: Comparison of detected frequency modes expressed as a percentage of all detected frequency modes in test specimens

N [%]	Bottom side degraded				Upper side degraded			
	Bottom surface hit		Upper surface hit		Bottom surface hit		Upper surface hit	
	Upper sensor	Bottom sensor	Upper sensor	Bottom sensor	Upper sensor	Bottom sensor	Upper sensor	Bottom sensor
	25	100	56	69	56	88	44	63

For comparison of all conducted measurements setup we can interpreted the effectivity of each setup by expressing the number of successfully localized frequency modes in each setup, with reference to setup with highest stable frequency count and lowest damping ratios. At the Table 3 each setup is present with relative percentage of successfully detected frequencies.

It seems that, best position for testing was setup, where receiving sensor was placed on the bottom flat side of the test specimen, and the hits took place on the same flat side. Other variants of testing resulted in less obtainable information in terms of stable frequency modes.

Conclusion

Designed experiment enabled application of experimental modal analysis as effective method for evaluation of structural integrity. The change of frequency modes is mainly caused by ongoing hydration process in the test specimens, which caused a slight 10-15% increase in all frequencies in both long term cycling. This leads to main conclusions:

- hydration process continued even in QUV chamber, and strong UV radiation did not significantly affect the mechanical properties such as frequency modes or damping ratios,
- there was observed more chaotic behaviour in frequency modes shift after the degradation, where specific frequency modes could not be detected at some of the testing points of test grids,
- during the interpretation phase the most effective position of receiving accelerometer was at the flat bottom surface of the test specimens, without difference if top rough surface or bottom flat surface of specimens was exposed to UV radiation,
- the change in frequency modes indicates a change in inner integrity, where first three frequency modes are not constant at all test points of test specimens, as was in the initial state before degradation.

The conducted experiment also helped to set the basic conditions for testing of small-scale mortar test specimens by experimental modal analysis.

Acknowledgment

This paper has been worked out under the project Czech Science Foundation GACR No. GA 19-04703S supported by Czech Science Foundation and the project No. LO1408 "AdMaS UP - Advanced Materials, Structures and Technologies", supported by Ministry of Education, Youth and Sports under the „National Sustainability Programme I”.

Reference

- [1] K. Scrivener and R. Kirkpatrick, "Innovation in use and research on cementitious material", *Cement and Concrete Research*, vol. 38, no. 2, pp. 128-136, 2008.
- [2] J. Damtoft, J. Lukasik, D. Herfort, D. Sorrentino and E. Gartner, "Sustainable development and climate change initiatives", *Cement and Concrete Research*, vol. 38, no. 2, pp. 115-127, 2008.
- [3] J. Crow, "The concrete conundrum", *Chemistry World*, pp. 62-66, 2008.
- [4] "Major countries in worldwide cement production from 2014 to 2018", *Statista*. [Online]. Available: <https://www.statista.com/statistics/267364/world-cement-production-by-country/>. [Accessed: 2020-01-22].
- [5] V. Glukhovskiy, "Soil silicates.", vol. 1959.
- [6] A. Palomo, P. Krivenko, I. Garcia-Lodeiro, E. Kavalerova, O. Maltseva and A. Fernández-Jiménez, "A review on alkaline activation: new analytical perspectives", *Materiales de Construcción*, vol. 64, no. 315, 2014.
- [7] *Alkali Activated Materials*. Dordrecht, 2014.
- [8] T. Luukkonen, Z. Abdollahnejad, J. Yliniemi, P. Kinnunen and M. Illikainen, "One-part alkali-activated materials: A review", *Cement and Concrete Research*, vol. 103, pp. 21-34, 2018.

- [9] "QUV ACCELERATED WEATHERING TESTER". [Online]. Available: <https://www.q-lab.com/products/quv-weathering-tester/quv>. [Accessed: 2020-03-08].
- [10] T. Guo and X. Weng, "Evaluation of the freeze-thaw durability of surface-treated airport pavement concrete under adverse conditions", *Construction and Building Materials*, vol. 206, pp. 519-530, 2019.
- [11] D. Ewins, *Modal testing: theory, practice, and application*, 2nd ed. Philadelphia, PA: Research Studies Press, 2000.
- [12] A. Brandt, *Noise and vibration analysis: signal analysis and experimental procedures*. Chichester: Wiley, 2011.
- [13] A. Arda Ozdemir and S. Gumussoy, "Transfer Function Estimation in System Identification Toolbox via Vector Fitting", *IFAC-PapersOnLine*, vol. 50, no. 1, pp. 6232-6237, 2017.
- [14] X. Bao, H. Sun, G. Iglesias, T. Wang and C. Shi, "Signal denoising method for modal analysis of an offshore platform", *Journal of Loss Prevention in the Process Industries*, vol. 63, 2020.
- [15] P. Welch, „The use of fast Fourier transform for the estimation of power spectra: A method based on time averaging over short, modified periodograms.“ *IEEE Transactions on Audio and Electroacoustics*. 1967, 15(2), 70-73. ISSN 0018-9278. doi:10.1109/TAU.1967.1161901
- [16] G. Tondreau and A. Deraemaeker, "Numerical and experimental analysis of uncertainty on modal parameters estimated with the stochastic subspace method", *Journal of Sound and Vibration*, vol. 333, no. 18, pp. 4376-4401, 2014.
- [17] M. W. M. a. R. J. SZCZEPAŃSKI, „MODAL ANALYSIS OF REAL TIMBER FRAME HOUSES WITH DIFFERENT INSULATION MATERIALS,“ *Advances in Science and Technology Research Journal*, pp. 215-221, 2016.
- [18] G. Ivan and B. Moor, "Subspace identification combined with new mode selection techniques for modal analysis of an airplane", *IFAC Proceedings Volumes*, vol. 36, no. 16, pp. 675-680, 2003.
- [19] Heylen W., S. Lammens and P. Sas. „Modal Analysis Theory and Testing“, *KULeuven* (ISBN 90-73802-61-X), 1998.
- [20] A. OZDEMIR, A. and S. GUMUSSOY, „Transfer Function Estimation in System Identification Toolbox via Vector Fitting“, *IFAC-PapersOnLine*. 2017, 50(1), 6232-6237. ISSN 24058963. doi:10.1016/j.ifacol.2017.08.1026
- [21] H. Vold, K. Napolitano and D. Hensley. „Aliasing in Modal Parameter Estimation.“ *SAE 2007 Transactions Journal of Passenger Cars: Mechanical Systems*. 2007, 2007-05-15, V116(6), 11. ISSN 0148-7191.
- [22] X. Li, J. He, M. Li, H. Jiang and Y. Huang, "Modal analysis method for tensegrity structures via stiffness transformation from node space to task space", *Engineering Structures*, vol. 203, 2020.
- [23] H. Šimonová, B. Kucharczyková, V. Bílek, L. Topolář and D. Kocáb, „Influence of curing conditions on mechanical and fracture properties of alkali activated slag concrete“, *IOP Conference Series: Materials Science and Engineering*. 2019, 660. ISSN 1757-899X. doi:10.1088/1757-899X/660/1/012004